



HAL
open science

Pervasive detachment faults within the slow spreading oceanic crust at the poorly coupled Antilles subduction zone

Boris Marcaillou, Frauke Klingelhofer, Muriel Laurencin, Jean-Frédéric Lebrun, Mireille Laigle, Serge Lallemand, Laure Schenini, Aurélien Gay, Milton Boucard, Kingsley Ezenwaka, et al.

► To cite this version:

Boris Marcaillou, Frauke Klingelhofer, Muriel Laurencin, Jean-Frédéric Lebrun, Mireille Laigle, et al.. Pervasive detachment faults within the slow spreading oceanic crust at the poorly coupled Antilles subduction zone. *Communications Earth & Environment*, 2021, 2, pp.203. 10.1038/s43247-021-00269-6 . hal-03360100

HAL Id: hal-03360100







<https://hal.science/hal-03360100>

Submitted on 30 Sep 2021

HAL is a multi-disciplinary open access archive for the deposit and dissemination of scientific research documents, whether they are published or not. The documents may come from teaching and research institutions in France or abroad, or from public or private research centers.

L'archive ouverte pluridisciplinaire **HAL**, est destinée au dépôt et à la diffusion de documents scientifiques de niveau recherche, publiés ou non, émanant des établissements d'enseignement et de recherche français ou étrangers, des laboratoires publics ou privés.

Pervasive detachment faults within the slow spreading oceanic crust at the poorly coupled Antilles subduction zone

Boris Marcaillou ¹, Frauke Klingelhoefer ², Muriel Laurencin ³, Jean-Frédéric Lebrun⁴, Mireille Laigle ¹, Serge Lallemand⁵, Laure Schenini¹, Aurélien Gay⁵, Milton Boucard ⁴, Kingsley Ezenwaka¹ & David Graindorge⁶

Oceanic crust formed at slow-spreading ridges is currently subducted in only a few places on Earth and the tectonic and seismogenic imprint of the slow-spreading process is poorly understood. Here we present seismic and bathymetric data from the Northeastern Lesser Antilles Subduction Zone where thick sediments enable seismic imaging to greater depths than in the ocean basins. This dataset highlights a pervasive tectonic fabric characterized by closely spaced sequences of convex-up Ridgeward-Dipping Reflectors, which extend down to about 15 km depth with a 15-to-40° angle. We interpret these reflectors as discrete shear planes formed during the early stages of exhumation of magma-poor mantle rocks at an inside corner of a Mid-Atlantic Ridge fracture zone. Closer to the trench, plate bending could have reactivated this tectonic fabric and enabled deep fluid circulation and serpentinization of the basement rocks. This weak serpentinized basement likely explains the very low interplate seismic activity associated with the Barbuda-Anegada margin segment above.

¹ Université Côte d'Azur, CNRS, Observatoire de la Côte d'Azur, IRD, Géoazur, Valbonne, France. ² IFREMER, Dpt. of Marine Geosciences, Plouzané, France. ³ Université de Lille, CNRS, Univ. Littoral Côte d'Opale, UMR 8187, LOG, Laboratoire d'Océanologie et de Géosciences, Lille, France. ⁴ Géosciences Montpellier, Université de Montpellier, CNRS, Université des Antilles, Pointe à Pitre, Guadeloupe(FWI). ⁵ Geosciences Montpellier, Université de Montpellier, CNRS, Université des Antilles, Montpellier, France. ⁶ Geosciences Océan, UMR 6538, Université Bretagne Occidentale, Institut Universitaire Européen de la Mer, Plouzané, France. ✉email: boris.marcaillou@geoazur.unice.fr

Oceanic basement formed at slow-spreading mid-ocean ridges (MORs), exhibits remarkable variations in crustal thickness, seismic velocity and tectonic fabric, as previously inferred from bathymetric data^{1–3}, paleomagnetic studies^{4,5} sampling and drilling of outcrops of deep-seated rocks^{6,7} and numerical modelling^{8,9}. In contrast, few seismic data image this fabric variability at depth^{10–13}. Poorly sedimented seafloor near MORs causes severe scattering of seismic waves during mapping expeditions, which impedes accurate intra-crustal imaging at depth¹⁴. As a result, deciphering the complex variability of oceanic tectonic fabric in seismic images remains challenging.

This variability, from magmatically robust to tectonically dominated segments, depends on the spreading rate and the relative contribution of tectonic extension and magmatic diking to oceanic spreading^{8,9}. At magmatically robust segments, oceanic spreading is mainly taken up by vigorous melt delivery, which leads to typical velocity-depth “Penrose” structure of extrusive basalts overlying intrusive gabbros¹⁵. In contrast, tectonically dominated spreading favors stretched and thinned crust possibly hosting widely spaced, long-lived, low-angle, rideward-dipping detachment faults¹⁶, exhuming serpentinized peridotites with a varying amount of gabbro bodies. This heterogeneous crustal composition is referred to as the “plum-pudding model”^{17,18}. The velocity-depth structure then usually consists of one layer with a rather constant velocity gradient^{19–21} depending on a decreasing serpentinization degree with depth²². Reston et al.¹¹ argue that more closely spaced faulting may result from a tectonic sequence where a detachment fault forms, slips, flexes and becomes inactive when a new detachment fault develops nearby. However, in the absence of convincing deep seismic images for such tectonic sequences, the model of widely spaced detachment faults frequently prevails.

New bathymetric and multichannel seismic (MCS) data, collected in the NLA trench during cruises ANTITHESIS 1 and 3^{23,24} call into question this generic model for the first time. The sedimentary layer reduces the scattering, allowing up-to-6-s-two-way-traveltime (stwt) deep seismic imaging, which is unprecedented for slow-spreading oceanic basement. These data reveal impressive along-strike variations in oceanic fabric, showing an unexpected deep and pervasive tectonic pattern within the basement created at a segment end of the Mid-Atlantic Ridge. These images challenge the long-lived detachment model, highlight that the tectonic imprint of slow-spreading onto the oceanic basement has possibly been underestimated, and raise questions about the seismic consequences of subduction of tectonically dominated, hydrated, serpentinized, and weak oceanic basement patches.

Results and discussion

Oceanic tectonic pattern near the Jacksonville Fracture zone.

The ~N120°-trending Jacksonville Fracture Zone extends from the Northwestern Atlantic to the NLA Subduction Zone²⁵ (Fig. 1). To the south, the 15–20 Fracture Zone subducts beneath the margin at a convergence rate of 20 mm/yr in the N254°E direction²⁶. Between these fracture zones, the Cretaceous oceanic basement in the trench (Fig. 1A) ages westward²⁷. Based on the 300–330 km distance between chron C34 (83 Ma) and C32 (71.6 Ma)²⁸, the mean half-spreading rate was low, 26–29 mm/yr, at the spreading center.

The Jacksonville Patch, originated from the ridge segment end close to the Jacksonville Fracture Zone, is currently located in the trench between 18 and 19°N. The bathymetry and deep structure within this patch drastically differs from that of the incoming oceanic plate in neighboring zones.

To the southeast and the northwest of this patch, the oceanic fabric of the incoming plate corresponds to ~N20°-trending

elongated topographic highs sub-parallel to the magnetic anomalies (Fig. 1B, Supplementary Fig. 1). In addition, in every seismic line perpendicular to the trench (Ant01 07, 10, 11, 12, 14, and 50) reflectors of the seafloor, oceanic sediments, and the basement top step down westward along steep fault planes that dominantly dip toward the margin (Fig. 2A). These normal faults penetrate the basement down to gently southwestward-dipping discontinuous reflections *M*, 1.9 to 2.2 stwt beneath the top of the basement, interpreted as the Moho. These faults crop out at bathymetric scarps, directed N100–120°E, sub-parallel or slightly oblique to the deformation front.

This margin sub-parallel faulting in the outer trench wall has long been described as the result of the incoming plate bending into the subduction zone^{29,30}. According to these studies, plate bending mainly reactivates inherited tectonic structures of the oceanic fabric when favorably oriented (sub-parallel to the trench) and produces new faults when the fabric is highly oblique with respect to the trench. Offshore of the NLA, the oceanic fabric trends at more than 70° angle to the trench. The southwestward-dipping faults, sub-parallel to the deformation front, are thus likely to be newly formed plate bending faults.

Within the Jacksonville Patch, the bathymetric map and associated dip and strike seismic lines (Ant06, 43, 44, 45, 52, 53, and 54) show a drastically different tectonic pattern in the trench (Fig. 1B, Supplementary Fig. 1B). The smoother seafloor is neither spiked with the N20°-trending ridges of the oceanic fabric, nor deformed by the margin-subparallel scarps of plate-bending normal faults. In contrast, short, shallow and steep faults dipping toward east and west bound ~4–6 km wide grabens in the oceanic basement. These grabens define ~N100–110°-directed seafloor undulations trending at 40° angle to the margin front. The seismic lines do not show organized reflections at typical Moho depths. The most striking features are 5–10-km-spaced, convex-up, high-amplitude reflector sequences, which dip from the top of the oceanic basement down to 5 stwt below the seafloor (Fig. 2B). The sequences are 0.1–0.2-stwt-thick (200 to 500 m) and locally up-to-0.5-stwt-thick (1 to 1.5 km).

Rideward-Dipping oceanic-basement Reflectors (RDRs).

In order to estimate the true dip direction and geometry of these reflector sequences, we performed depth-conversion of MCS lines Ant45 and 53 interpretations (Fig. 3) as well as a pre-stack depth migration of line Ant45. We used a combined MCS / wide-angle seismic (WAS) velocity model based on nearby WAS line Ant06³¹ (Supplementary Fig. 3). In this model, the basement corresponds to a 5.6–6.5-km-thick single layer with a 5.5–7.4 km/s velocity range from top to bottom and a constant velocity gradient of 0.27 s⁻¹. Moreover, we used seismic attributes derived from seismic data in order to confirm the reflector sequences geometry. Computing RMS amplitude provides information about reflection physical properties and particularly fluid content³². This analysis suggests that the reflector sequences, compared to other intra-crustal reflections, show physical properties consistent with fluid-rich and/or serpentinized rocks within the upper 6 km of the oceanic basement. At greater depths, the dimming of reflections suggests a decreasing fluid content and/or serpentinization degree (Supplementary Fig. 4). The mean apparent dip angle increases from 17° to 25° in N125°E-trending line Ant53 and from 15° to 35° in N40°E-trending line Ant45 (Fig. 3A, Supplementary Fig. 5). These lines intersect each other (Fig. 3B) and reveal that the reflectors dip in a N60–90°E direction, towards the Mid-Atlantic Ridge, with a dip angle that increases from 20–30° in the upper 3 km, up to 45° between 3 and 8 km depth (Fig. 3C). We refer to these sequences as Rideward-Dipping oceanic-basement Reflectors (RDRs) (Fig. 4).

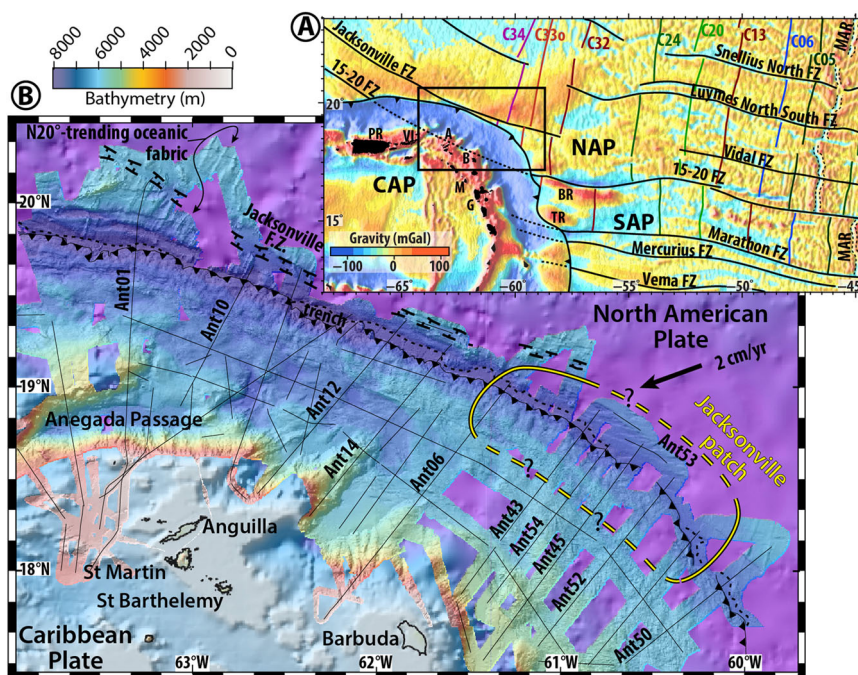


Fig. 1 Maps of the study area. **A** Satellite free-air gravity map⁶² showing fracture zones (solid lines), synthetic flow lines (colored lines), and the Mid-Atlantic Ridge (dotted lines) in the Central Atlantic for chrons 5 (8.9 Ma), 6 (19.4 Ma), 13 (35.3 Ma), 20 (44.7 Ma), 24 (55 Ma), 32 (71.6 Ma), 330 (80.2 Ma), and 34 (84 Ma)⁶³. A stands for Anegada, B for Barbuda, BR for Barracuda Ridge, CAP for Caribbean Plate, FZ for Fracture Zone, G for Guadeloupe, M for Montserrat, MAR for Mid-Atlantic Ridge, NAP for North American Plate, TR for Tiburon Ridge, PR for Puerto-Rico, SAP South American Plate, and VI for Virgin Island. The black frame refers to Fig. 1B. **B** Bathymetric map showing location for multichannel seismic lines labeled AntXX and the Jacksonville Fracture Zone (dashed black lines). Close-up on target zones are in Supplementary Fig. 1.

Previous seismic data depicted distant convex-up ridgeward-dipping reflectors with similar dipping angle at segment ends of slow-spreading ridges, interpreted as large-offset long-lived detachment faults, for instance in the Cretaceous-aged Eastern Central Atlantic^{11,13} and at the South West Indian Ridge (SWIR)¹⁰. At the SWIR, the faults are associated with similar ~0.5-stwt-thick sub-parallel bright discontinuous reflectors interpreted as damage zones. The RDRs are also partly consistent with closely spaced, ~1-km-thick sequences of convex-up LCRs (Lower-Crust ridgeward-dipping Reflectors) in the Northwestern Atlantic^{12,33} as well as in lower crust generated at the faster Mid-Pacific spreading ridge offshore of the Middle America Trench³⁴, Japan^{35–37}, Alaska³⁸, and Hawaii³⁹. These LCRs have been interpreted as lithological layering resulting from magma flow in the Atlantic³³ and the Pacific^{40,41}. However, discrete spacing of reflectors rather than pervasive layering more readily supports ductile shear zones^{37,42} due to spreading-related deep tectonic events¹² and/or anomaly in melt delivery at the mid-ocean ridge⁴².

The RDRs size and geometry partly differ from these analogues. These reflectors extend from the top of the oceanic basement to, at least, 6 km below (Fig. 3, Supplementary Fig. 5) while the LCRs are restricted to the lower crust and sole out downward onto the Moho. Discretely spaced thin sequences of subparallel RDRs are poorly consistent with pervasive and massive fan-shaped layering at Seaward Dipping Reflectors (SDRs) and lava flows. At last, the RDRs are closely spaced and most of them do not deform or fracture the top of the oceanic basement and the sediment layer, contrasting with the classical image of distant detachment faults¹¹ with topographic expressions³, in the Northeastern Atlantic. However, this fault spacing at a slow to intermediate spreading axis depends on the fraction of the plate separation rate that is accommodated by magmatic ridge-axis dyke intrusion⁸. According to these authors,

a tectonically dominated slow-spreading ridge segment with moderate magmatic activity can generate closely spaced detachment-type deformation zones during early stages of basement exhumation.

Based on this discussion, we propose that the Jacksonville Patch lithosphere consists of serpentinized mantle rocks, possibly hosting gabbro bodies exhumed along low-angle detachment systems¹⁶ or by serpentine diapirism up high-angle faults⁴³. Although we cannot rule out serpentine diapirism, inside corners of fracture zones are known to be prone to detachment faulting⁴⁴, the RDRs more readily image pervasive proto-detachment shear zones related to early tectonic extension at a magma-poor inside corner of the segmented MAR. In this interpretation, the RDRs more readily image pervasive proto-detachment shear zones related to early tectonic extension at a magma-poor inside corner of the segmented MAR. Approaching the trench, the plate bending, reactivates extensional strain along the RDRs, favoring fluid percolation, rock alteration and serpentinization, increasing acoustic impedance contrast and reflection amplitude. The RMS analysis supports this interpretation showing high RMS amplitude along the RDRs within the upper 6 km and at the top of the oceanic crust above the RDRs (Supplementary Fig. 4).

Seismogenic behavior of subducting serpentine-bearing rocks.

The NLA Subduction Zone has hosted only 39 thrust-faulting earthquakes, detected teleseismically ($M_w > 5$), with focal mechanisms compatible with interplate co-seismic slips since 1973 (Fig. 5). Most of these subduction-type events occurred to the North of Guadeloupe where they are aggregated in two seismicity clusters: from Montserrat to Barbuda and from the Anegada Passage to Virgin Island⁴⁵. Very few of them occurred along the ~110-km-wide margin segment in between and to the South of Guadeloupe.

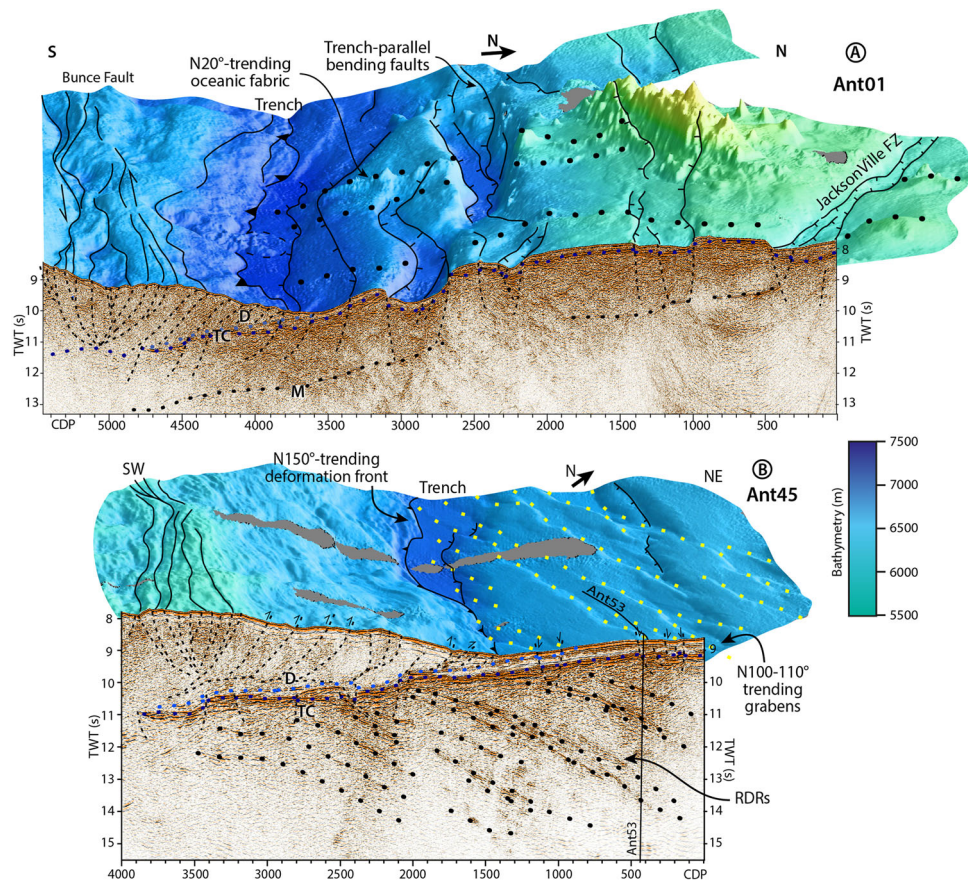


Fig. 2 3D seismic-bathymetry blocks at magmatically robust and tectonically dominated segments. Three-dimensional seismic-bathymetry views illustrating typical oceanic basement (**A** line Ant01) and the spectacular, tectonically dominated, exhumed oceanic basement (**B** line Ant45) located outside and inside the Jacksonville Patch, respectively. D, TC, and M stand for Decollement, Top of the oceanic Crust, and Moho, respectively. Black and yellow dotted lines underline the Ridgeward-Dipping oceanic-basement Reflectors (RDRs) and the oceanic grabens direction, respectively. Vertical Exaggeration 1:3.5. Additional 3D blocks are in Supplementary Fig. 2.

In the Southern and Central Lesser Antilles, numerous fracture zones in the subducting South American Plate (Fig. 1A) likely trigger deep crustal hydration and mantle serpentinization^{46–48}. This high water budget is prone to impede large interplate coseismic rupture, rather favoring alternate slip behavior (SSE, VLFE, EETS)⁴⁹ and/or numerous low-magnitude events^{46,48}. In contrast, in the NLA, the only fracture zone (the 15–20 FZ) of the subducting North American Plate to interact with the subduction zone (Fig. 1) has not subducted deep enough to favor dehydration of the subducting serpentinized mantle⁴⁷. This fracture zone, located at less than 30 km depth beneath the forearc³¹, could trigger shallow dewatering and margin tectonic deformation, weakening the interplate contact, reducing the seismic coupling and affecting the megathrust seismogenic behavior. However, the fracture zone underthrusts similarly the two clusters of subduction-type teleseisms ($M_w > 5$), and the gap in between (Fig. 5) suggesting a low influence onto the interplate seismicity in the NLA.

We propose that the reduced strength of the subducting plate basement at least partly made of serpentinized mantle rocks strongly contributes to the megathrust weakness and the interplate seismicity reduction. Low-temperature species of serpentine minerals, chrysotile, and lizardite have a low coefficient of internal friction, low fracture strength, and a nominally non-dilatant mode of brittle deformation, which favor localized slip on discrete surfaces, cataclastic flow by shear microcracking^{50–52}, and plastic flow within individual grains⁵³. This substantial weakening of serpentine-

bearing rocks is not a linear function of the degree of serpentinization but is similar in slightly hydrated peridotites and pure serpentinites²². The subduction of an heterogeneously faulted, hydrated and serpentinized basement is likely to generate an interplate patchiness of contrasting frictional properties, which may impede full interplate coupling⁵³, instead favoring a mix of stable and unstable behaviors prone to triggering small- M_w , slow-slip, and/or very-low frequency earthquakes⁵⁴. Similar conditions are suspected in anomalous non-seismic regions in locally hydrated forearc mantle within Northeast Japan⁵³.

The Lesser Antilles is an end-member subduction zone, which undergoes the subduction of highly hydrated fracture zones and unsuspected large-scale tectonically dominated oceanic patches. Our data depict for the first time pervasive and closely spaced proto-detachment shear planes, reactivated by the plate bending in the trench within the oceanic basement, at least partly made of serpentinized mantle rocks exhumed at a former inside corner of the MAR. The landward extent of this patch is unclear beyond 40 km from the deformation front, because of seismic amplitude loss at great depth. However, downdip, tectonic interaction and fluid circulation between the patch and the 15–20 Fracture Zone possibly alter the forearc strength. Thus, the reduced strength and fluid circulation related to the Jacksonville serpentinized basement, its pervasive tectonic fabric, and the proximity of the hydrated 15–20 Fracture Zone are likely to account for the heterogeneous distribution of subduction earthquakes in the NLA.

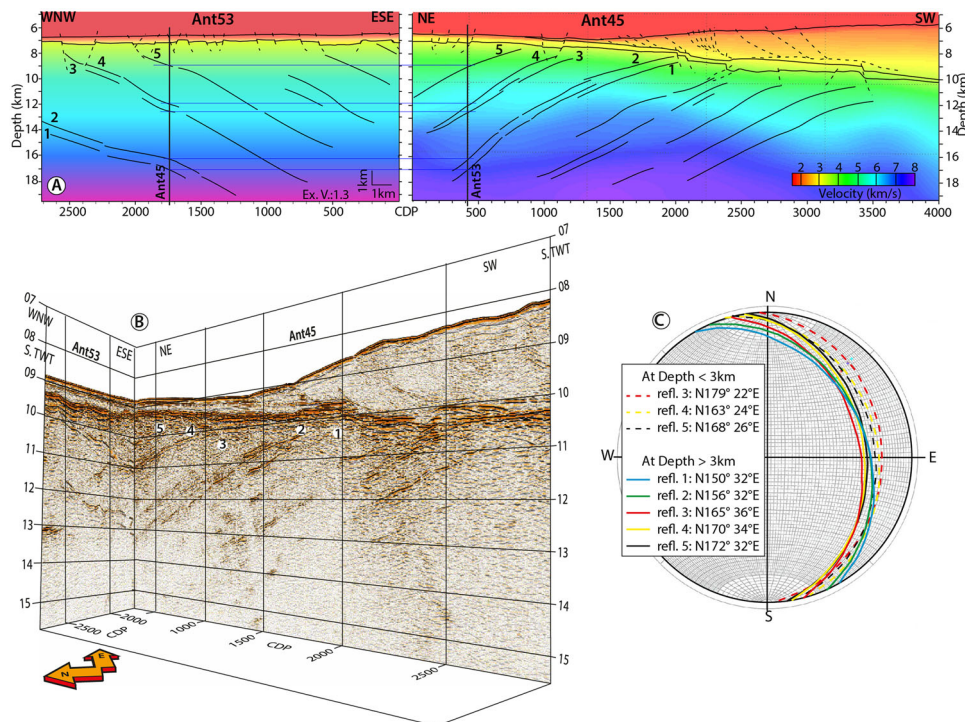


Fig. 3 Geometry and direction of Ridgeward Dipping Reflectors. Depth-converted interpretation for lines Ant45 and Ant53 (A), 3D view in time section (B), and Schmidt diagram (C) reveal that the convex-up sequences of RDRs in the oceanic basement dip toward the Mid Atlantic Ridge. Lines location is in Figs. 1B and 3D bathymetry-seismic view for lines Ant45 and Ant53 are in Fig. 2B and Supplementary Fig. 2, respectively. Figure 4 shows an interpreted perspective view of the RDRs.

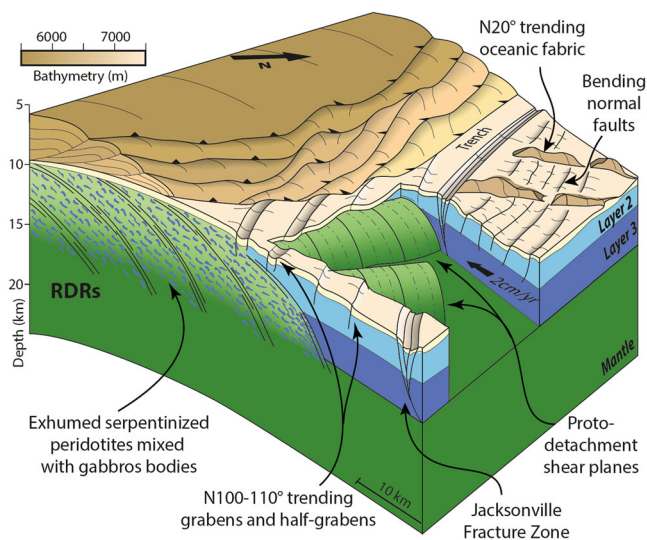


Fig. 4 Interpreted 3D view of the tectonically dominated slow-spreading basement subducting beneath the Northern Lesser Antilles Subduction Zone. Perspective view showing the structural transition of the Atlantic basement from the inside to the outside corner of the Jacksonville Fracture Zone. The Jacksonville patch at the inside corner consists of serpentinitized mantle rock possibly mixed with gabbro bodies exhumed along proto-detachment shear planes which formed at a tectonically dominated magma poor ridge segment end. These detachments, reactivated while subducting beneath the NLA draw Ridgeward Dipping Reflectors (RDRs) in along-dip vertical sections.

Methods

Data acquisition. Our results are based on recent multichannel seismic (MCS) wide-angle (WAS) seismic and bathymetric data collected during cruises ANTITHESIS 1²³ and ANTITHESIS 3²⁴. Multibeam swath bathymetry data were

recorded using a Kongsberg EM122 and a RESON Seabat7150 (432 – 880 beams echosounders) during ANTITHESIS 1 and 3, respectively. We recorded MCS lines Ant01, 10.2 and 12 during Antithesis 1²³, using a 7699 cu in 18-elements airgun seismic source towed at 17-m-depth and a 3-km-long streamer composed of 288 channels spaced at 12.5 m and towed at 20-m-depth. We acquired lines Ant45, 50, 53, and 54 during Antithesis 3²⁴, using a 6500 cu in, 16-elements airgun seismic source towed at 14-m-depth and a 4.5-km-long streamer composed of 720 channels spaced at 6.25 m and towed at 15-m-depth. Shots were fired every 75 m providing a 30-fold coverage.

Data processing. Swath processing consists in spikes and excessive slopes removal by automatic procedure and manual ping editing using *Caribes*[®] and *Globe*[®] softwares (IFREMER). Digital terrain models were produced with a grid spacing of 75 m. Vertical accuracy is between a few meters and tens of meters depending on depth. Bathymetric and slope maps were calculated and processed using *QGis*. Maps reveal reliefs in the order of tens of meters high and few hundred meters apart.

MCS data processing includes quality control, binning, band-pass filtering, fK filtering, external and internal mutes, noise attenuation, predictive deconvolution, multiple suppression, velocity analysis, normal move out and dip move out corrections, stacking and pre-stack time migration, using *Solid-QC*[®] (Ifremer) and *Geovation*[®] (CGG-Veritas) Softwares⁵⁵. We performed iterative Prestack Kirchhoff time migration (PSTM) to yield optimal migration velocities and form the final prestack migrated images. PSTM results in focusing correctly seismic energy from genuine basement reflections but not from out-of-planes arrivals from seafloor or basement propagating through regions of lower root-mean-square velocity. Thus, any intra-basement event observed on presented PSTM images can be interpreted as true reflection.

Depth-converted interpretation and depth-migrated seismic data. Converting and/or migrating to depth the seismic images is a mandatory condition to address the questions of the geometry, dipping angle, and orientation of the RDRs. The depth of investigation (11 to 18 km) is much larger than the streamer length (4 and 4.5 km for Antithesis 1 and 3, respectively). At great depth, this relative shortness of the streamers results in high uncertainties in interval velocity model strictly inferred from Normal-Move-Out (NMO) velocities. In order to reduce this uncertainty, we build composite velocity models based on MCS lines Ant45 and 53 and WAS line Ant06³¹ (Supplementary Fig. 3), located within the Jacksonville Patch 70 km to the northwest. These models consists in: 1/ NMO velocities converted to interval velocities using the Dix formula at shallow depth (i.e., from the seafloor to the topmost hundreds of milliseconds in the subducting basement) and

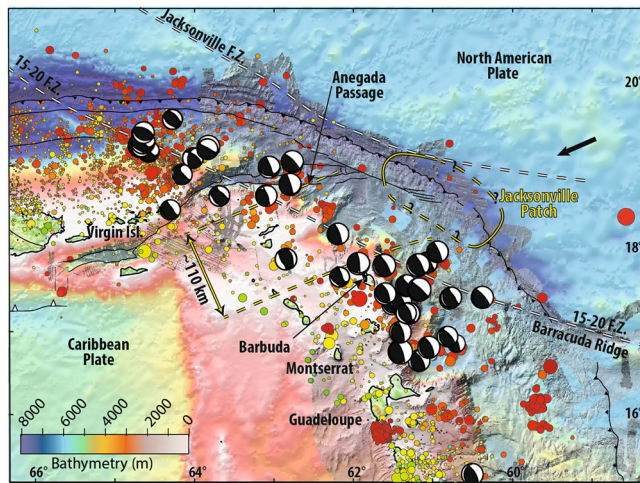


Fig. 5 Seismicity map. Map view of the seismic activity in the Northern Lesser Antilles. The circles represent the earthquakes from the EHB catalogue and the USGS PDE, sized by magnitude and colored by depth. Black focal mechanisms are thrust earthquakes from the gCMT catalogue, aggregated in two clusters separated by a 110-km large quiet zone (dashed yellow lines). Dashed white lines indicate the 15-20 and Jacksonville Fracture Zones.

2/ velocities inferred from first-arrival traveltimes tomography for line Ant06 at greater depth in the basement and the mantle. We then base our investigations on two complementary methodological approaches. We convert to depth the interpretation for seismic lines An45 and 53 (Fig. 3) using these combined MCS/WAS velocity models. In order to confirm this conversion, MCS line Ant45 is migrated to depth (Supplementary Fig. 5) with a preserved amplitude Pre-Stack Depth Migration (PSDM) approach^{56–60} performed in the angle domain. The velocity macro-model is iteratively corrected during migration, using the “migration-velocity-analysis” approach⁶¹ until Common Image Gathers (CIG) show flat reflections. When this condition is satisfied, the CIG are stacked, providing an increased accuracy for the migrated image. In this methodological approach, it is noteworthy that parallel lines Ant45 and 06 are located 70 km from each other. As a result, the PSDM of line Ant45 should be considered as an additional constraint for the RDRs geometry complementing the rougher depth conversion, more than as a robust image for the deep structure of the subduction zone. Despite this uncertainty, both methods result in similar location, depth, geometry, and dipping angles for the RDRs. These reflectors are slightly deeper and steeper in the depth-converted image than in the interpreted PSDM MCS line.

RMS amplitude analysis. Seismic amplitude attributes analysis is commonly used in basin and oil exploration in order to identify and delineate structural and stratigraphic features associated with fluid-rich intervals³². The Root Mean Square (RMS), based on reflection coefficient, independently from the reflection polarity, is particularly suited for fluid content analysis. The RMS amplitude A_{RMS} is calculated from original signal amplitudes $a_i(t)$ over a time window of N samples indexed with i , using the « Petrel » software (Schlumberger):

$$A_{RMS} = \frac{1}{N} \sum_i (a_i(t))^2$$

As a result, this analysis estimates the signal overall amplitude and describes the signal average amplitude within a time window.

Data availability

Every geophysical data of the ANTITHESIS cruises are available on the internet site of the French Oceanographic Fleet (<https://campagnes.flotteoceanographique.fr/search>). Interested readers write/select “Antithesis” in field “search campaign” and the desired data set in field “Data Managed by SISMER.” Once every needed data set is selected, the readers can download it from “My basket” page.

Code availability

Seismic data processing used softwares *SolidQC* (Ifremer) and *Geovation* (CGG), bathymetric data were processed with softwares *Globe* and *Claritas* (Ifremer). We used *Kingdom Suite* for the RMS analysis. Maps and 3D bathymetric views were drafted using *GMT*, *Qgis*, and *Adobe Illustrator*. The ray-Born PSDM code derives from an original private version by P. Thierry and G. Lambaré (Mines School of Paris) and the Migration-

velocity analysis code, from the original version by W. Agudelo and A. Ribodetti (Geoazur).

Received: 28 January 2021; Accepted: 8 September 2021;
Published online: 30 September 2021

References

- Cann, J. R. et al. Corrugated slip surfaces formed at ridge–transform intersections on the Mid-Atlantic Ridge. *Nature* **385**, 329 (1997).
- Sauter, D. et al. Continuous exhumation of mantle-derived rocks at the Southwest Indian Ridge for 11 million years. *Nat. Geosci.* **6**, 314–320 (2013).
- Smith, D. K., Cann, J. R. & Escartin, J. Widespread active detachment faulting and core complex formation near 13 degrees N on the Mid-Atlantic Ridge. *Nature* **442**, 440–443 (2006).
- Garcés, M. & Gee, J. S. Paleomagnetic evidence of large footwall rotations associated with low-angle faults at the Mid-Atlantic Ridge. *Geology* **35**, 279 (2007).
- Morris, A. et al. Footwall rotation in an oceanic core complex quantified using reoriented Integrated Ocean Drilling Program core samples. *Earth Planet. Sci. Lett.* **287**, 217–228 (2009).
- MacLeod, C. J. et al. Direct geological evidence for oceanic detachment faulting: the Mid-Atlantic Ridge, 15°45'N. *Geology* **30**, 879–882 (2002).
- Schroeder, T. & John, B. E. Strain localization on an oceanic detachment fault system, Atlantis Massif, 30°N, Mid-Atlantic Ridge. *Geochem. Geophys. Geosyst.* **5**, Q11007 (2004).
- Buck, W. R., Lavier, L. L. & Poliakov, A. N. B. Modes of faulting at mid-ocean ridges. *Nature* **434**, 719–723 (2005).
- Tucholke, B. E., Behn, M. D., Buck, W. R. & Lin, J. Role of melt supply in oceanic detachment faulting and formation of megamullions. *Geology* **36**, 455 (2008).
- Momoh, E., Cannat, M., Watremez, L., Leroy, S. & Singh, S. C. Quasi-3-D seismic reflection imaging and wide-angle velocity structure of nearly amagmatic oceanic lithosphere at the ultraslow-spreading Southwest Indian Ridge. *J. Geophys. Res.* **122**, 9511–9533 (2017).
- Reston, T. J. & Ranero, C. R. The 3-D geometry of detachment faulting at mid-ocean ridges. *Geochem. Geophys. Geosyst.* **12**, <https://doi.org/10.1029/2011gc003666> (2011).
- Morris, E. et al. Seismic structure of oceanic crust in the western North Atlantic. *J. Geophys. Res.* **98**, 13, 879–813,903 (1993).
- Ranero, C. R. & Reston, T. J. Detachment faulting at ocean core complexes. *Geology* **27**, 983–986 (1999).
- Peirce, C., Sinha, M., Topping, S. & Gill, C. Morphology and genesis of slow-spreading ridges-seabed scattering and seismic imaging within the oceanic crust. *Geophys. J. Int.* **168**, 59–89 (2007).
- White, R. S., McKenzie, D. & O’Nions, R. K. Oceanic crustal thickness from seismic measurements and rare earth element inversions. *J. Geophys. Res.* **97**, 19683–19715 (1992).
- Smith, D. K. Tectonics: mantle spread across the sea floor. *Nat. Geosci.* **6**, 247–248 (2013).
- Cannat, M. How thick is the magmatic crust at slow spreading oceanic ridges? *J. Geophys. Res.* **101**, 2847–2857 (1996).
- Ildefonse, B. et al. Oceanic core complexes and crustal accretion at slow-spreading ridges. *Geology* **35**, 623 (2007).
- Dean, S. M., Minshull, T. A., Whitmarsh, R. B. & Loudon, K. E. Deep structure of the ocean-continent transition in the southern Iberia Abyssal Plain from seismic refraction profiles: the IAM-9 transect at 40°20'N. *J. Geophys. Res.* **105**, 5859–5885 (2000).
- Grevemeyer, I. et al. Episodic magmatism and serpentinized mantle exhumation at an ultraslow-spreading centre. *Nat. Geosci.* **11**, 444–448 (2018).
- Van Avendonk, H. J. A. et al. Seismic velocity structure of the rifted margin of the eastern Grand Banks of Newfoundland, Canada. *J. Geophys. Res.* **111**, 1–26 (2006).
- Escartin, J., Hirth, G. & Evans, B. Strength of slightly serpentinized peridotites: implications for the tectonics of oceanic lithosphere. *Geology* **29**, 1023–1026 (2001).
- Marcaillou, B. & Klingelhoefer, F. ANTITHESIS-1-Leg1 Cruise, RV L’Atalante, <https://doi.org/10.17600/13010070> (2013).
- Marcaillou, B. & Klingelhoefer, F. ANTITHESIS-3 Cruise, RV Pourquoi Pas? <https://doi.org/10.17600/16001700> (2016).
- Bouysse, P., Garcia-Reyes, A., Mercier de Lépinay, B. & Pubellier, M. (CCGM/CGMW, 2020).
- DeMets, C., Gordon, R. G. & Argus, D. F. Geologically current plate motions. *Geophys. J. Int.* **181**, 1–80 (2010).

27. Müller, R. D., Royer, J.-Y., Cande, S. C., Roest, W. R. & Maschenkov, S. *Caribbean Basins. Sedimentary Basins of the World 4* (ed Mann, P.) (Elsevier Science B.V. 1999).
28. Cande, S. C. & Kent, D. V. Revised calibration of geomagnetic polarity timescale for the late Cretaceous and Cenozoic. *J. Geophys. Res.* **100**, 6093–6095 (1995).
29. Masson, D. G. Fault patterns at outer trench walls. *Marine Geophys. Res.* **13**, 209–225 (1991).
30. Ranero, C. R., Phipps Morgan, J., McIntosh, K. D. & Reichert, C. Bending-related faulting and mantle serpentinization at the Middle America trench. *Nature* **425**, 367–373 (2003).
31. Laurencin, M., Graindorge, D., Klingelhoefer, F., Marcaillou, B. & Evain, M. Influence of increasing convergence obliquity and shallow slab geometry onto tectonic deformation and seismogenic behavior along the Northern Lesser Antilles zone. *Earth Planet. Sci. Lett.* **492**, 59–72 (2018).
32. Chopra, S. & Marfurt, K. J. Seismic attributes – a historical perspective. *Geophysics* **70**, 3SO–28SO (2005).
33. McCarthy, J., Mutter, J. C., Morton, J. L., Sleep, N. H. & Thompson, G. A. Relic magma chamber structures preserved within the Mesozoic North Atlantic crust? *GSA Bulletin* **100**, 1423–1436 (1988).
34. Hallenborg, E., Harding, A. J. & Kent, G. M. Seismic structure of 15 Ma oceanic crust formed at an ultrafast spreading East Pacific rise: evidence for kilometer-scale fracturing from dipping reflectors. *J. Geophys. Res.* **108**, <https://doi.org/10.1029/2003jb002400> (2003).
35. Kodaira, S. et al. Seismological evidence of mantle flow driving plate motions at a palaeo-spreading centre. *Nat. Geosci.* **7**, 371–375 (2014).
36. Ranero, C. R., Reston, T. J., Belykh, I. & Gribidenko, H. Reflective oceanic crust formed at a fast spreading center in the Pacific. *Geology* **25**, 499–502 (1997).
37. Reston, T. J., Ranero, C. R. & Belykh, I. The structure of Cretaceous oceanic crust of the NW Pacific: constraints on processes at fast spreading centers. *J. Geophys. Res.* **104**, 629–644 (1999).
38. Bécel, A., Shillington, D. J., Nedimović, M. R., Webb, S. C. & Kuehn, H. Origin of dipping structures in fast-spreading oceanic lower crust offshore Alaska imaged by multichannel seismic data. *Earth Planet. Sci. Lett.* **424**, 26–37 (2015).
39. Eittrheim, S. L. et al. Oceanic crustal thickness and seismic character along a central Pacific transect. *J. Geophys. Res.* **99**, 3139–3145 (1994).
40. Henstock, T. J., Woods, A. W. & White, R. S. The accretion of oceanic crust by episodic sill intrusion. *J. Geophys. Res.* **98**, 4143–4161 (1993).
41. Phipps Morgan, J. & Chen, Y. J. The genesis of oceanic crust: magma injection, hydrothermal circulation, and crustal flow. *J. Geophys. Res.* **98**, 6283–6297 (1993).
42. Han, S. et al. Seismic reflection imaging of the Juan de Fuca plate from ridge to trench: new constraints on the distribution of faulting and evolution of the crust prior to subduction. *J. Geophys. Res.* **121**, 2015JB012416 (2016).
43. Zhou, H. & Dick, H. J. B. Thin crust as evidence for depleted mantle supporting the Marion rise. *Nature* **494**, 195–200 (2013).
44. Reston, T. J. et al. A rifted inside corner massif on the Mid-Atlantic Ridge at 5°S. *Earth Planet. Sci. Lett.* **200**, 255–269 (2002).
45. Hayes, G. P., McNamara, D. E., Seidman, L. & Roger, J. Quantifying potential earthquake and tsunami hazard in the lesser Antilles subduction zone of the Caribbean region. *Geophys. J. Int.* **196**, 510–521 (2013).
46. Paulatto, M. et al. Dehydration of subducting slow-spread oceanic lithosphere in the Lesser Antilles. *Nat. Commun.* **8**, (2017).
47. Cooper, G. F. et al. Variable water input controls evolution of the Lesser Antilles volcanic arc. *Nature* **582**, 525–529 (2020).
48. Schlaphorst, D. et al. Water, oceanic fracture zones and the lubrication of subducting plate boundaries—insights from seismicity. *Geophys. J. Int.* **204**, 1405–1420 (2016).
49. Saffer, D. M. & Tobin, H. J. Hydrogeology and mechanics of subduction zone forearcs: fluid flow and pore pressure. *Annu. Rev. Earth Planet. Sci.* **39**, 157–186 (2011).
50. Escartín, J., Hirth, G. & Evans, B. Nondilatant brittle deformation of serpentinites: implications for Mohr-Coulomb theory and the strength of faults. *J. Geophys. Res.* **102**, 2897–2913 (1997).
51. Moore, D. E., Lockner, D. A., Shengi, M., Summers, R. & Byerlee, J. D. Strengths of serpentinite gouges at elevated temperature. *J. Geophys. Res.* **102**, 14714–787801 (1997).
52. Reinen, L. A. Seismic and aseismic slip indicators in serpentinite gouge. *Geology* **28**, 135–138 (2000).
53. Hirauchi, K.-I., Katayama, I., Uehara, S., Miyahara, M. & Takai, Y. Inhibition of subduction thrust earthquakes by low-temperature plastic flow in serpentine. *Earth Planet. Sci. Lett.* **295**, 349–357 (2010).
54. Saffer, D. M. & Wallace, L. M. The frictional, hydrologic, metamorphic and thermal habitat of shallow slow earthquakes. *Nat. Geosci.* **8**, 594–600 (2015).
55. Laurencin, M. et al. The polyphased tectonic evolution of the Anegada Passage in the northern Lesser Antilles subduction zone. *Tectonics* **36**, <https://doi.org/10.1002/2017TC004511> (2017).
56. Lambaré, G., Operto, S., Podvin, P. & Thierry, P. 3D ray+born migration/inversion - part 1: theory. *Geophysics* **68**, 1348–1356 (2003).
57. Lambaré, G., Virieux, J., Madariaga, R. & Jin, S. Iterative asymptotic inversion in the acoustic approximation. *Geophysics* **57**, 1138–1154 (1992).
58. Operto, S., Xu, S. & Lambaré, G. Can we quantitatively image complex structures with rays. *Geophysics* **65**, 1223–1238 (2000).
59. Thierry, P., Lambaré, G., Podvin, P. & Noble, M. 3D preserved amplitude prestack depth migration on a workstation. *Geophysics* **64**, 222–229 (1999).
60. Ribodetti, A., Operto, S., Agudelo, W., Collot, J.-Y. & Virieux, J. Joint ray+born least-squares migration and simulated annealing optimization for high-resolution target-oriented quantitative seismic imaging. *Geophysics* **76**, <https://doi.org/10.1190/1.3554330> (2011).
61. Al-Yahya, K. M. Velocity analysis by iterative profile migration. *Geophysics* **54**, 718–729 (1989).
62. Sandwell, D. T. & Smith, W. H. F. Slope correction for ocean radar altimetry. *J. Geodesy* **88**, 765–771 (2014).
63. Müller, R. D. & Roest, W. R. Fracture zones in the North Atlantic from combined Geosat and Seasat data. *J. Geophys. Res.* **97**, 3337–3350 (1992).

Acknowledgements

We thank the captain and crew of the R/Vs “*L’Atalante*” and “*Pourquoi Pas?*” for the data acquisition during marine surveys ANTITHESIS 1 and 3. M.B.’s PhD Thesis was funded by the Regional Council of Guadeloupe. M.Lau.’s PhD thesis was funded by The Regional Council of Bretagne. We gratefully acknowledge S. Sambolian, S. Operto, and A. Ribodetti for providing the optimized version of the PSDM code, and A. Ribodetti for adapting the codes to the MCS data of this study. Special thanks to Marc-Andre Gutscher for revising the English and providing us with insightful comments.

Author contributions

B.M. supervised the data processing and wrote the manuscript. B.M., F.K., and J.-F.L. conceived the ANTITHESIS project and were Principal Investigators onboard RVs “*L’Atalante*” and “*Pourquoi Pas?*”. L.S. and J.-F.L. supervised the seismic and multibeam onboard processing, respectively. M.Lau., M.B., and K.E. performed the post-cruise seismic processing during their PhD, supervised by B.M., D.G., J.-F.L., F.K., M.Lai., and S.L. A.G. performed RMS analyses. All authors participated in the Antithesis cruises, discussed the scientific issues, and commented on the manuscript.

Competing interests

The authors declare no competing interests.

Additional information

Supplementary information The online version contains supplementary material available at <https://doi.org/10.1038/s43247-021-00269-6>.

Correspondence and requests for materials should be addressed to Boris Marcaillou.

Peer review information *Communications Earth & Environment* thanks Harm Van Avendonk and the other, anonymous, reviewer(s) for their contribution to the peer review of this work. Primary Handling Editors: Luca Dal Zilio, Joe Aslin. Peer reviewer reports are available.

Reprints and permission information is available at <http://www.nature.com/reprints>

Publisher’s note Springer Nature remains neutral with regard to jurisdictional claims in published maps and institutional affiliations.



Open Access This article is licensed under a Creative Commons Attribution 4.0 International License, which permits use, sharing, adaptation, distribution and reproduction in any medium or format, as long as you give appropriate credit to the original author(s) and the source, provide a link to the Creative Commons license, and indicate if changes were made. The images or other third party material in this article are included in the article’s Creative Commons license, unless indicated otherwise in a credit line to the material. If material is not included in the article’s Creative Commons license and your intended use is not permitted by statutory regulation or exceeds the permitted use, you will need to obtain permission directly from the copyright holder. To view a copy of this license, visit <http://creativecommons.org/licenses/by/4.0/>.

© The Author(s) 2021